

Stress transfer along the western boundary of the Bayan Har Block on the Tibet Plateau from the 2008 to 2020 Yutian earthquake sequence in China

Ke Jia¹, Shiyong Zhou², Jiancang Zhuang³, and Changsheng Jiang⁴

¹Northwestern Polytechnical University

²Peking University

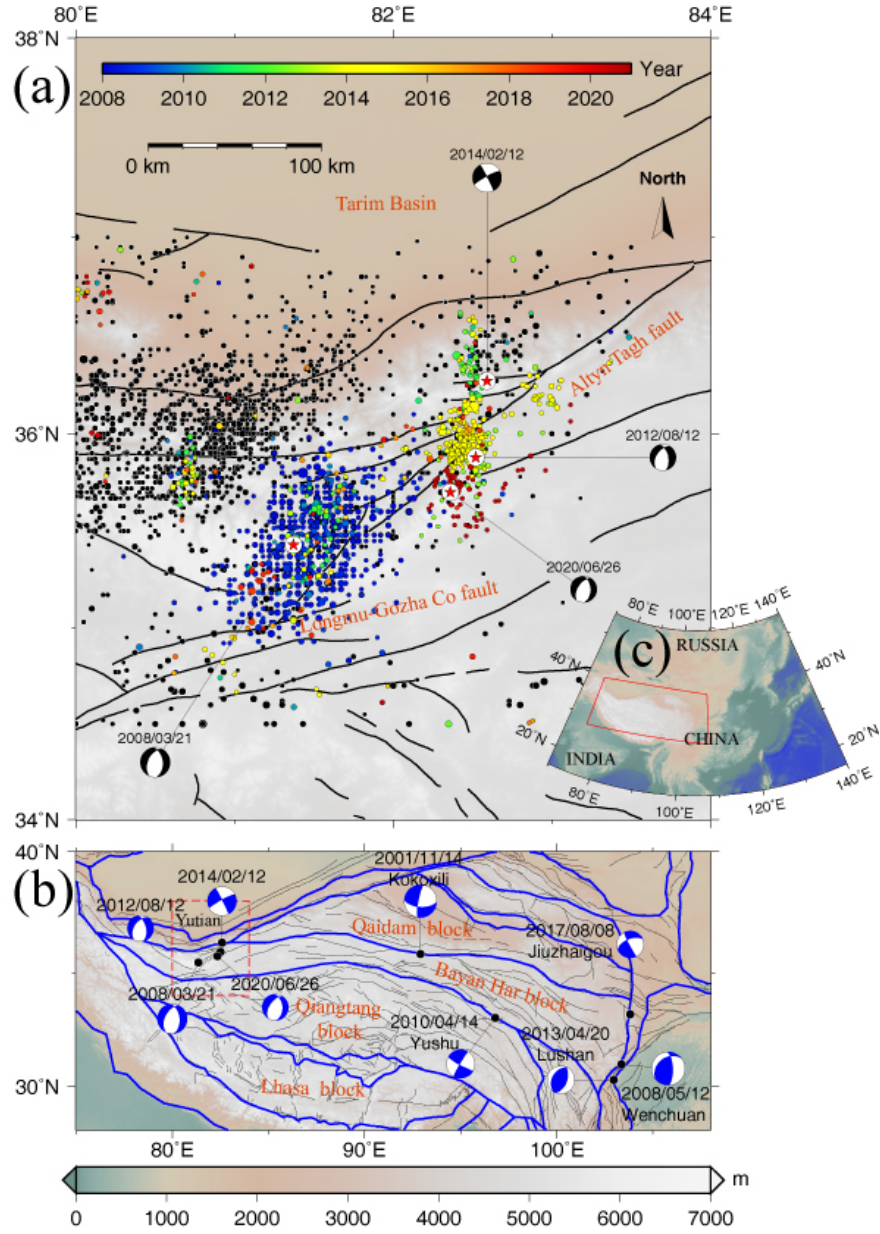
³Institute of Statistical Mathematics

⁴China Earthquake Administration

November 24, 2022

Abstract

Eight M_L[?]7.0 earthquakes have occurred around the Bayan Har block, NW Tibet, China, since 2000, resulting in a large number of casualties and countless economic loss. Near the western boundary of the Bayan Har block, four M_L[?]6.0 Yutian earthquakes have occurred from 2008 to 2020. Stress interactions among them are comprehensively investigated by applying the ETAS (Epidemic-Type Aftershock Sequence) model and calculating (Coulomb failure stress change). The viscoelastic induced by proceeding Yutian earthquakes on hypocenters of the 2012, 2014 and 2020 Yutian earthquakes are -1.5004×10^{-4} , 3.5820×10^{-3} and 1.4770×10^{-1} MPa, respectively. The background probabilities of the 2008, 2012, 2014 and 2020 Yutian earthquakes are 0.87, 0.97, 1.5×10^{-3} and 8.7×10^{-5} , respectively. Combining those two independent approaches, we conclude that the 2008 and 2012 Yutian earthquakes are more like background earthquakes and that the 2014 and 2020 Yutian earthquakes were triggered by the proceeding Yutian earthquakes.



1 **Stress transfer along the western boundary of the Bayan**
2 **Har Block on the Tibet Plateau from the 2008 to 2020 Yutian**
3 **earthquake sequence in China**

4
5 Ke Jia^{1*}, Shiyong Zhou^{2*}, Jiancang Zhuang³, Changsheng Jiang⁴

6
7 1 School of Automation, Northwestern Polytechnical University, Xi'an 710129, China

8 2 School of Earth and Space Sciences, Peking University, Beijing 100871, China

9 3 The Institute of Statistical Mathematics, 10-3 Midori-Cho, Tachikawa, Tokyo 190-8562,
10 Japan

11 4 Institute of Geophysics, China Earthquake Administration, No.5 Minzu Daxue Nan Road,
12 Haidian District, Beijing 100086, China

13 *Corresponding authors: jk@nwpu.edu.cn, zsy@pku.edu.cn

14
15 **Key points:**

- 16 1. Four $M_I \geq 6.0$ have occurred on the western boundary of the Bayan Har block, NW Tibet,
17 China, from 2008 to 2020.
- 18 2. The 2008 Yutian earthquake may have contributed to the occurrences of the 2014 and 2020
19 Yutian events due to stress triggering.
- 20 3. Statistical insights provide a good cross reference for the triggering mechanism due to small
21 uncertainties.

28 **Abstract**

29 Eight $M \geq 7.0$ earthquakes have occurred around the Bayan Har block, NW Tibet, China, since
30 2000, resulting in a large number of casualties and countless economic loss. Near the western
31 boundary of the Bayan Har block, four $M \geq 6.0$ Yutian earthquakes have occurred from 2008 to
32 2020. Stress interactions among them are comprehensively investigated by applying the ETAS
33 (Epidemic-Type Aftershock Sequence) model and calculating ΔCFS (Coulomb failure stress
34 change). The viscoelastic ΔCFS induced by proceeding Yutian earthquakes on hypocenters of
35 the 2012, 2014 and 2020 Yutian earthquakes are -1.5004×10^{-4} , 3.5820×10^{-3} and 1.4770×10^{-1}
36 MPa, respectively. The background probabilities of the 2008, 2012, 2014 and 2020 Yutian
37 earthquakes are 0.87, 0.97, 1.5×10^{-3} and 8.7×10^{-5} , respectively. Combining those two
38 independent approaches, we conclude that the 2008 and 2012 Yutian earthquakes are more like
39 background earthquakes and that the 2014 and 2020 Yutian earthquakes were triggered by the
40 proceeding Yutian earthquakes.

41

42 **Plain Language Summary**

43 Along the boundaries of the Bayan Har block, NW Tibet, China, there have been eight large
44 earthquakes since 2000, resulting in a large number of casualties and countless economic loss.
45 At its western boundary (Yutian region), four earthquakes with local magnitudes larger than 6.0
46 have occurred since 2008. Whether these four large earthquakes were triggered is an important
47 question in assessing regional seismic hazards. We combine two methods to address this issue.
48 One is direct calculation of stress transfer and the other is estimation of the probabilities of
49 them being background events (an event is driven by tectonic loading). We find that the stress
50 transfer from proceeding major earthquakes to the 2012 Yutian earthquake is smaller than the
51 earthquake triggering threshold (0.01 MPa), while those of the 2014 and 2020 Yutian
52 earthquakes were moderate compared with the triggering threshold. The background
53 probabilities of the 2008 and 2012 Yutian earthquakes are high (close to 1.0), while background
54 probabilities of the 2014 and 2020 Yutian earthquakes are very low (close to 0.0). Thus, we
55 conclude that the 2008 and 2012 Yutian earthquakes are more like background earthquakes and
56 that the 2014 and 2020 Yutian earthquakes were triggered by the proceeding Yutian earthquakes.

57

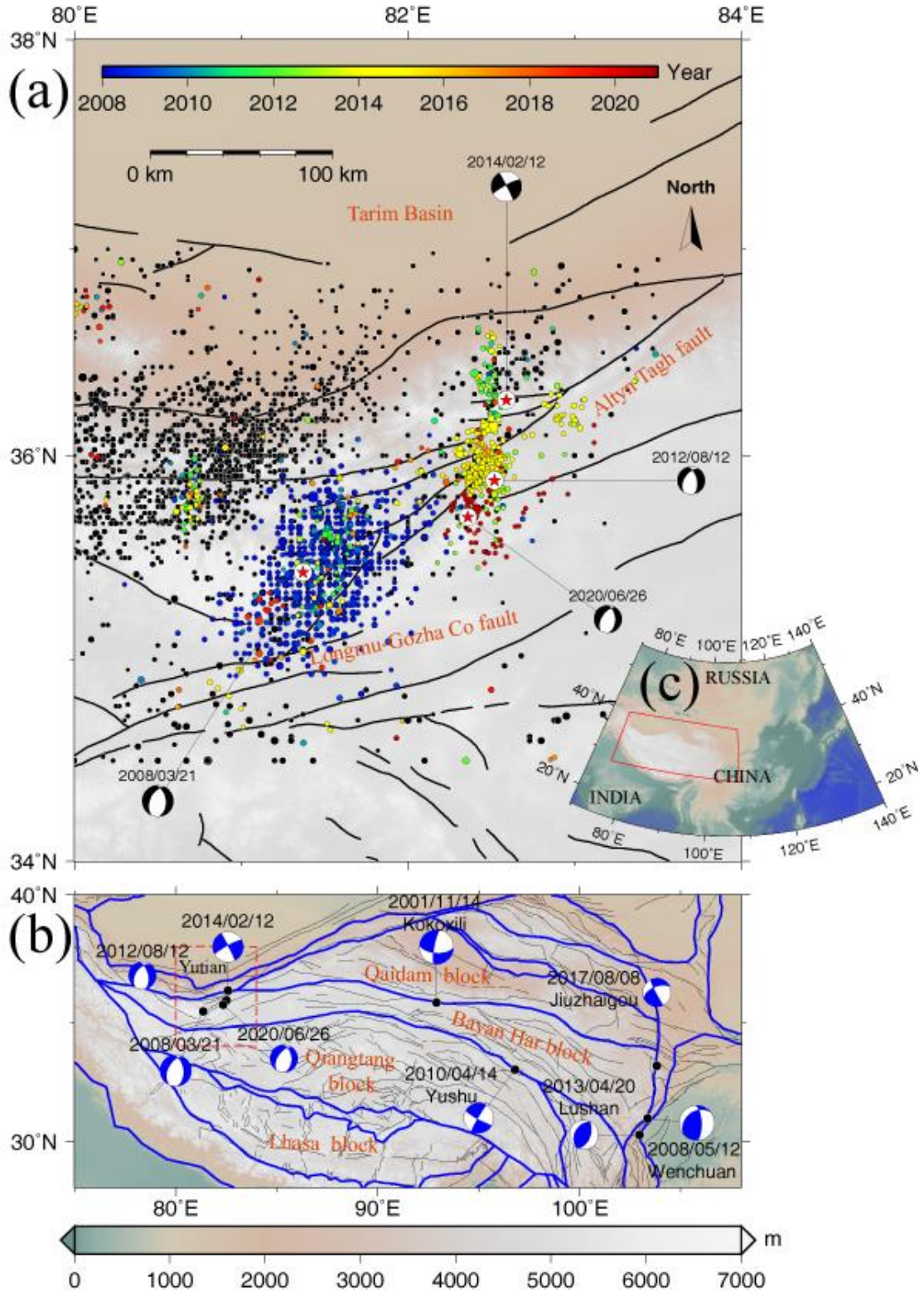
58 **1. Introduction**

59 Stress interactions among major earthquakes have received increasing attention. A number of
60 case studies (e.g., the 1992 Landers and 1999 Hector Mine earthquakes in the US (*Freed and*
61 *Lin*, 2001); the 2008 Wenchuan, 2013 Lushan and 2017 Jiuzhaigou earthquakes in China (*Jia*
62 *et al.*, 2014; *Jia et al.*, 2018; *Wan and Shen*, 2010; *Wang et al.*, 2014b); the 2010-2011
63 Canterbury Earthquake Sequence in New Zealand (*Quigley et al.*, 2016); and the foreshock and
64 mainshock of the 2019 Ridgecrest earthquake in the US (*Pope and Mooney*, 2020; *Ramos et*
65 *al.*, 2020)) have been investigated under the framework of the Coulomb failure hypothesis,
66 which assumes that positive ΔCFS promotes the occurrence of earthquakes and negative
67 ΔCFS delays them. In addition, many researchers have shown that the calculated ΔCFS are
68 positively correlated with observed seismicity rate changes (*Harris*, 1998; *Jia et al.*, 2014; *Kroll*
69 *et al.*, 2017; *Pollitz and Cattania*, 2017; *Stein*, 1999; *Toda et al.*, 2012; *Toda et al.*, 2005; *Zhuang*
70 *et al.*, 2005). This indicates that observed seismicity increases in regions with positive ΔCFS
71 and decreases in regions with negative ΔCFS values. However, several studies have found
72 that earthquakes still occurred in a stress shadow (*Harris and Simpson*, 1996; *Jia et al.*, 2018;
73 *Parsons*, 2002), which cannot be explained by the Coulomb failure hypothesis. Earthquake
74 triggering mechanisms have also been investigated in previous studies (*Freed*, 2005).
75 Coseismic slip (*McCloskey et al.*, 2005), postseismic deformation (e.g., afterslip (*Cattania et*
76 *al.*, 2015), viscoelastic relaxation of the lower crust and upper mantle (*Freed and Lin*, 2001)),
77 dynamic seismic waves (*Gomberg et al.*, 2001) and fluid-involved processes (e.g., poroelastic
78 rebound) (*Hughes et al.*, 2010; *Tung and Masterlark*, 2018) could contribute to triggering
79 earthquakes. Remote triggering of earthquakes at great distances could be well explained by
80 dynamic triggering due to the passage of seismic waves, while distinguishing local triggering
81 in the near field between static and dynamic stress changes could be a challenge (*Meng and*
82 *Peng*, 2014). In this way, calculations of ΔCFS and seismicity rate changes could help to
83 clarify stress interactions between earthquakes and faults and further evaluate seismic hazards.

84

85 The recent June 26 (GMT+8), 2020 Mw 6.3 Yutian earthquake (hereafter 20YT) occurred in
86 the western Kunlun Mountains, NW Tibet, China. Three other $M \geq 6.0$ earthquakes have

87 occurred near the epicenter of the 20YT since 2008. The March 20, 2008 Mw 7.1 Yutian
88 earthquake (hereafter 08YT), one of the largest normal earthquakes on the continents, occurred
89 94 km to the west of the epicenter of the 20YT. The August 12, 2012 Mw 6.2 Yutian earthquake
90 (hereafter 12YT) and the February 12, 2014 Mw 6.9 Yutian earthquake (hereafter 14YT)
91 occurred 25 km and 61 km to the north of the epicenter of the 20YT (Figure 1). The source
92 region of these four earthquakes on the western boundary of the Bayan Har block experiences
93 an extensive stress field bounded by two strike-slip fault systems: the Altyn Tagh fault in the
94 north and the Longmu-Gozha Co fault in the south (*Taylor and Yin, 2009*), which further relates
95 to the collision of the Indian plate and Eurasian plate. This area is the intersection of multiple
96 groups of large strike-slip active fault belts with different strikes. The 08YT, 12 YT, 14 YT and
97 20YT sequences provide an opportunity for a case study of the Coulomb failure hypothesis and
98 help to evaluate the seismic hazard of the Bayan Har block.
99



100

101 Figure 1 Tectonic settings of the Yutian region and Bayan Har block. (a) The black filled circles
 102 represent earthquakes with $M \geq 3.5$ from 1 January 1970 to 31 December 2007 (from China
 103 Earthquake Data Center, <http://data.earthquake.cn/index.html>). The color filled circles are
 104 earthquakes with $M \geq 3.5$ from 1 January 2008 to 23 August 2020, and colors represent their

105 occurrence time. The four red stars represent the epicenters of the 2008, 2012, 2014 and 2020
106 Yutian earthquakes, and their focal mechanisms are from the Global Centroid Moment Tensor
107 (GCMT, <https://www.globalcmt.org/CMTsearch.html>). The black lines represent major faults
108 (*Zhang et al.*, 2003). (b) Nine major earthquakes ($M \geq 7.0$ except for the Yutian region) have
109 occurred on the boundaries of the Bayan Har block since 2000. The red dashed polygon
110 represents the region of (a). (c) The red solid polygon represents the region of (b) with respect
111 to mainland China.

112

113 Previous studies have shown stress triggering between the 08YT and 14YT (*Li et al.*, 2015;
114 *Wang et al.*, 2017; *Zhao et al.*, 2016) and seismicity rate changes following the 08YT, 12YT
115 and 14YT (*Jiang et al.*, 2014; *Zhao et al.*, 2016). Using a three-dimensional viscoelastic finite
116 element model, *Li et al.* (2015) showed that ΔCFS induced by the 08YT on the slip direction
117 of the 14YT exceeded 0.01 MPa (the earthquake triggering threshold) (*Harris*, 1998;
118 *Reasenbergs and Simpson*, 1992). They implied an apparent triggering effect of the 08YT to
119 14YT and suggested that the 14YT had advanced 21.4-24.9 years from the 08YT (*Li et al.*,
120 2015). *Zhao et al.* (2016) claimed that the 14YT was located in the triggering zone caused by
121 the 08YT, and the observed spatial distributions of aftershocks of these two major events were
122 well correlated with positive ΔCFS distribution. *Wang et al.* (2017) examined coseismic,
123 postseismic and interseismic ΔCFS induced by the 08YT on the 14YT hypocenter and found
124 a triggering relationship between them. *He et al.* (2020) calculated the coseismic ΔCFS from
125 the 08YT, 12YT and 14YT and found that the 20YT falls in the positive Coulomb stress region,
126 suggesting that previous events promoted the 20YT.

127

128 However, the roles of the 12YT in stress interactions with other Yutian earthquakes and
129 postseismic stress changes on the hypocenter of the 20YT have not been investigated. More
130 importantly, whether the occurrence of the 20YT was triggered by preceding Yutian
131 earthquakes or a background event may lead to different evaluations of regional seismic hazards.
132 If the 20YT was a triggered event, the local stress level may still be in a condition of postseismic
133 release or adjustment. On the other hand, an independent 20YT implies continuous tectonic

134 loading and release. Especially for a relatively small region, occurrences of four $M \geq 6.0$
135 earthquakes within 13 years are rare and provide an opportunity to study static stress
136 interactions (elastic and viscoelastic stress changes) among them. Furthermore, together with
137 seismicity analysis, these two independent kinds of evidence could be useful to understand the
138 occurrence of the 20YT and seismic hazards in the Bayan Har block.

139

140 In this study, we comprehensively investigate the seismicity rate changes in the Yutian region
141 from 2008 to 2020, the ΔCFS at the hypocenter of the 20YT induced by the proceeding Yutian
142 earthquakes (08YT, 12YT and 14YT), and the correlations between them. The ETAS model
143 and stochastic declustering method are used to obtain the background seismicity rate change.
144 The coseismic (elastic) and postseismic (viscoelastic) ΔCFS are calculated in an
145 elastic/viscoelastic layered half-space. The uncertainties of ΔCFS are investigated by
146 considering different friction coefficients. Based on the results of ΔCFS and seismicity
147 analysis, we infer that the 08YT may have contributed to the occurrence of the 14YT and 20YT
148 due to stress triggering.

149

150 **2. Detection of seismicity rate changes by using the ETAS model**

151 2.1 Space-time ETAS model

152 The space-time ETAS model, proposed by *Ogata* (1998), combines several classic statistical
153 laws in seismicity, including the Omori-Utsu law, productivity law and Gutenberg-Richter law.
154 The ETAS model assumes that each earthquake could trigger its own aftershocks with an ability
155 corresponding to its magnitude. The ETAS model has been successfully applied in many
156 regions and has become a standard model to analyze spatial and temporal seismicity (*Jia et al.*,
157 2014; *Jia et al.*, 2018; *Ogata*, 2004; *Ogata and Zhuang*, 2006; *Zhuang et al.*, 2005; *Zhuang et*
158 *al.*, 2004). Details of the space-time ETAS model can be found in *Ogata and Zhuang* (2006).

159

160 After obtaining final estimations of parameters of the ETAS model, the background probability
161 (an event is regarded as a background event with a probability) of the j th event φ_j , can be
162 estimated by

163
$$\varphi_j = \frac{\mu(x_j, y_j)}{\lambda(t_j, x_j, y_j)}, \quad (1)$$

164 where $\mu(x_j, y_j)$ is the background and total seismicity rate at the location of j th event and
 165 $\lambda(t_j, x_j, y_j)$ is the total seismicity rate at the location and occurrence time of j th event.

166

167 2.2 Fitting ETAS model

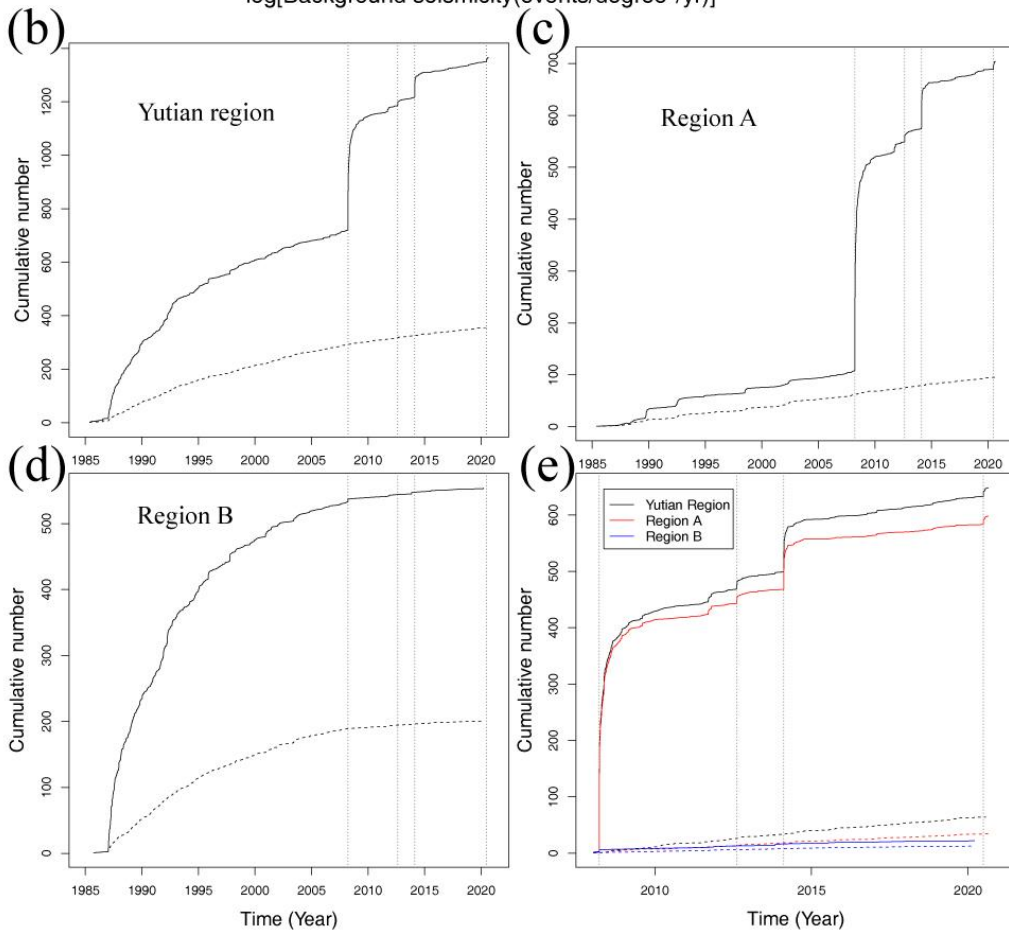
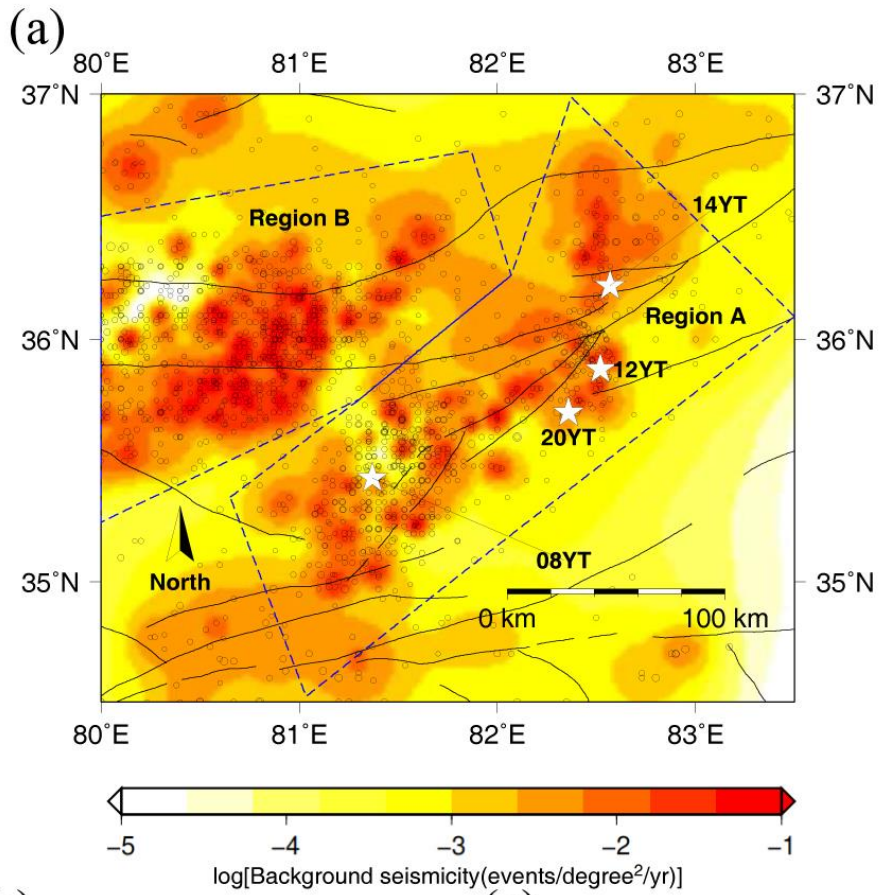
168 The catalog used in this study was downloaded from the China Earthquake Data Center (CEDC,
 169 <http://data.earthquake.cn/index.html>). A polygon region (80.0°-83.5°E, 34.5°-37.0°N) is
 170 selected to present the Yutian region for model fitting and seismicity analysis, and events above
 171 the cutoff magnitude were selected within the spatiotemporal range to fit the ETAS model by
 172 the maximum likelihood method. The time range is from 1 January 1980 to 23 August 2020,
 173 and the complete magnitude is approximately 3.5 from 1980 to 2020 (Figure S2), and we set
 174 the cutoff magnitude to 3.5. Details of the complete magnitude check are presented in the
 175 Supporting Information. The final estimations of the model parameters for the Yutian region
 176 are $\hat{A} = 0.382$ (events), $\hat{c} = 0.037$ (day), $\hat{\alpha} = 1.163$ (m⁻¹), $p = 1.178$, $\hat{D} = 1.46 \times 10^{-2}$
 177 (deg²), $\hat{q} = 2.396$, and $\hat{\gamma} = 0.211$ (m⁻¹).

178

179 2.3 Background seismicity rate in the Yutian region

180 The background probabilities of earthquakes with $M_w \geq 6.0$ are listed in Table S1, and the
 181 spatiotemporal distributions of the background probabilities are shown in Figure S3. From
 182 Figure S3, a number of aftershocks have been effectively distinguished. The spatiotemporal
 183 distributions of background probabilities are not sensitive to different intervals of background
 184 probabilities (Figure S3a-S3d). The background probabilities of 08YT, 12YT, 14YT and 20YT
 185 are 0.87, 0.97, 1.5×10^{-3} and 8.7×10^{-5} , respectively. This implies that the 08YT and 12YT are
 186 more like background earthquakes and that the 14YT and 20YT are triggered events in view of
 187 the ETAS model.

188



190 Figure 2 (a) Estimated spatial background seismicity in the Yutian region. Black circles
 191 represent earthquakes with magnitudes larger than 3.5 from 1970 to 2020. Four white stars
 192 indicate the 08YT, 12YT, 14YT and 20YT. Black lines are active faults. Regions A and B are
 193 marked with blue dashed lines for seismicity analysis. Note that the background seismicity rate
 194 is represented by the logarithm scale. (b)-(e) Cumulative number of earthquakes and
 195 background probabilities for the Yutian region (b), region A (c) and region B (d) marked in
 196 Figure 2(a). (e) A zoomed in view of seismicity changes from 2008 to 2021. The solid lines
 197 represent cumulative numbers of earthquakes in the study region and the dashed line represents
 198 the cumulative number of background probabilities. The four vertical dashed lines indicate the
 199 occurrence times of the 08YT, 12YT, 14YT and 20YT from left to right.

200

201 The spatial background seismicity is shown in Figure 2a. The epicenters of the 08YT, 12YT,
 202 14YT and 20YT suffer the highest background seismicity (approximately 0.1 $M \geq 3.5$
 203 events/degree²/yr), where the fault traces are also dense. The spatial background seismicity in
 204 the Yutian region shows a relatively high level resulting from the complex stepover zone with
 205 multiple normal faults (*Bie and Ryder, 2014; Tapponnier et al., 2001; Xu et al., 2013*).

206

207 The cumulative background probabilities of earthquakes $S(t)$, proposed by *Zhuang et al.*
 208 (2005), are written as

209
$$S(t) = \sum_{t_j < t} \varphi_j \quad (2)$$

210 We assume that the background seismicity rate is time-invariant in a stable region, thus $S(t)$
 211 constantly increases with time. Changes in the slope of the $S(t)$ curve imply changes in the
 212 background seismicity rate: an increased slope represents an activation of the background
 213 seismicity and a decreased slope indicates background quiescence.

214

215 Figure 2b-2e shows the cumulative number of earthquakes and background probabilities in the
 216 Yutian region and two subregions marked in Figure 2a. From [错误!未找到引用源。](#) a Figure
 217 2b-2e, it can be seen that the cumulative number of earthquakes in the Yutian region

218 dramatically increases after each major earthquake, while the rate of background probability
 219 remained stable from 1990 to 2020 and was not affected by the major earthquakes. This finding
 220 suggests that the Yutian region experiences constant background seismicity under a stable
 221 tectonic environment. The relationship between these four major Yutian earthquakes will be
 222 discussed later along with the calculations of ΔCFS . Region A indicates the fault zone of these
 223 four Yutian earthquakes, experiencing a constant background seismicity rate (错误!未找到引
 224 用源。 Figure 2c). Region B shows a decrease in background seismicity after the 08YT, which
 225 may have been caused by a negative ΔCFS induced by the 08YT (Figure 3a and 3d).

226

227 3. Coulomb Failure Stress change

228 To further investigate the stress interaction among the 2008, 2012, 2014 and 2020 Yutian
 229 earthquakes, we calculate the static (coseismic) and viscoelastic (postseismic) Coulomb stress
 230 changes induced by the preceding events using the numerical method of *Wang et al.* (2006).
 231 The lower crust and upper mantle are considered to be layered and viscoelastic. The proposed
 232 3D viscoelastic model contains an elastic upper crust, a viscoelastic lower crust with a
 233 viscosity of $1 \times 10^{18} Pa \cdot s$ and a viscoelastic upper mantle with a viscosity value of
 234 $1 \times 10^{20} Pa \cdot s$ (*Jia et al.*, 2012; *Wang et al.*, 2006; *Xiong et al.*, 2010). The layered rheological
 235 structure of the lithosphere is presented in the Supporting Information (Figure S4).

236

237 3.1 Method of calculation of ΔCFS

238 Given the shear stress change $\Delta \tau$ (positive in the sense of motion of the relevant fault) and
 239 the normal stress change $\Delta \sigma$ (positive for extension), ΔCFS can be calculated by (*Harris*,
 240 1998; *Steacy et al.*, 2005),

$$241 \quad \Delta CFS = \Delta \tau + \mu \left(\Delta \sigma - (\beta / 3) \sum \Delta \tau_{ii} \right) \quad (3)$$

242 where μ is the friction coefficient and β is Skempton's coefficient. If the medium is
 243 homogeneous and the fault zone materials are ductile, as discussed in *Harris* (1998) (formulas
 244 (3), (4) and (5) therein), ΔCFS can simply be calculated using

$$245 \quad \Delta CFS = \Delta \tau + \mu' \Delta \sigma \quad (4)$$

246 where μ' is the apparent coefficient of friction and $\mu' = \mu(1 - \beta)$.

247

248 Notably, the joint static and viscoelastic stress changes induced by the 2008/2012/2014 Yutian
249 earthquakes are considered in this study. Other possible mechanisms (e.g., dynamic stress
250 changes, stress changes driven by afterslips or fluid emigration), which may also contribute to
251 seismicity rate changes, have been neglected. The main mechanisms of postearthquake
252 deformation include viscoelastic relaxation of the lower crust and upper mantle and postseismic
253 afterslip on the fault plane. In the near field and the short period after the mainshock, the
254 postseismic deformation mainly comes from afterslip relaxing the stress perturbation by
255 localized deformation in the region of the fault plane (Agata *et al.*, 2019; Helmstetter and Shaw,
256 2009). In the far field and longterm after the mainshock, the viscoelastic relaxation of the lower
257 crust and upper mantle has a more significant contribution to postseismic deformation (He *et*
258 *al.*, 2018; Masuti *et al.*, 2016; Nur and Mavko, 1974; Peña *et al.*, 2020). Because of the long
259 distances between the epicenter of the 08YT and the epicenters of the other three Yutian
260 earthquakes, the contribution of afterslips induced by the 08YT is smaller than that of
261 viscoelastic relaxation of the lower crust and upper mantle. Poroelastic rebound, which refers
262 to coseismic stress changes that drive fluid flow from undrained conditions to drained
263 conditions, may also alter the local stress field after a major earthquake (Freed, 2007). However,
264 previous studies have shown that poroelastic rebound usually occurs within several months
265 (Hughes *et al.*, 2010; Jonsson *et al.*, 2003; Tung and Masterlark, 2018) and its contribution is
266 smaller than that of afterslip and viscoelastic relaxation processes (Peña *et al.*, 2020; Wang and
267 Fialko, 2018). Dynamic triggering due to the passage of seismic waves occurs hours and days
268 after the mainshock (Freed, 2005; Gomberg *et al.*, 2001; Hill and Prejean, 2007). Thus, the
269 poroelastic rebound process and dynamic triggering have been neglected in our study due to
270 much longer time intervals between these four Yutian earthquakes (4 to 12 years). In addition,
271 the impact of power-law rheology on viscoelastic relaxation has been investigated in recent
272 years (Agata *et al.*, 2019; Liu *et al.*, 2021; Peña *et al.*, 2019; 2020), and we apply linear
273 viscoelastic rheology in this study for simplicity. The application of power-law rheology needs
274 further investigation and is beyond our aims in this study.

275

276 3.2 Stress interactions among the four Yutian earthquakes

277 We have comprehensively investigated stress transfer among the 08YT, 12YT, 14YT and 20YT,
 278 which indicates that both static and viscoelastic ΔCFS induced by the proceeding Yutian
 279 earthquakes are calculated at the hypocenters of later Yutian earthquakes (Table 1). The
 280 coseismic slip model of the 2008 Yutian earthquake, provided by *Elliott et al.* (2010), is jointly
 281 inverted by the InSAR and body wave data. The coseismic slip model of the 2014 Yutian
 282 earthquake is estimated by inverting teleseismic data (*Zhang et al.*, 2014). The synthetic slip
 283 model 2012 Yutian earthquake is estimated based on the empirical relations of *Wells and*
 284 *Coppersmith* (1994) because of the lack of published coseismic slip models. The resolving
 285 depths of the 12YT, 14YT and 20YT are 15 km, 20 km and 15 km, respectively. The project
 286 planes are selected from focal mechanisms of the GCMT. The friction coefficient is set to 0.4,
 287 and Skempton's coefficient is set to 0.5.

288

289 Table 1 ΔCFS of the four major Yutian earthquakes (MPa)

290

	08YT		12YT		14YT		Proceeding Yutian earthquake
	coseismic	viscoelastic	coseismic	viscoelastic	coseismic	viscoelastic	Combined*
12YT	1.0×10^{-3}	-1.5×10^{-4}	\	\	\	\	-1.5×10^{-4}
14YT	-7.5×10^{-3}	2.6×10^{-3}	3.1×10^{-4}	9.6×10^{-4}	\	\	3.6×10^{-3}
20YT	3.0×10^{-3}	7.3×10^{-3}	3.5×10^{-2}	3.5×10^{-2}	1.1×10^{-1}	1.1×10^{-1}	1.5×10^{-1}

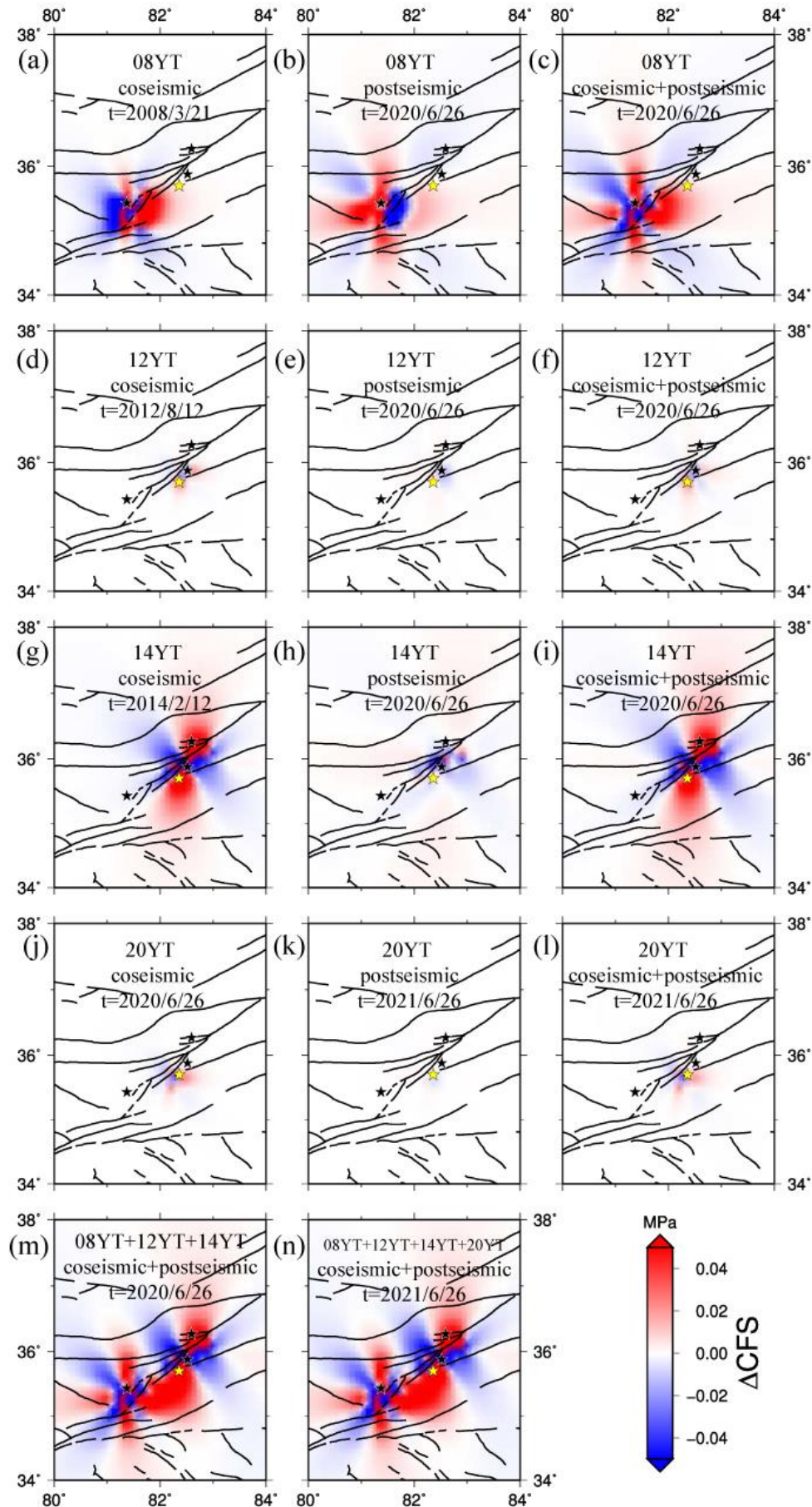
291 *"Combined" indicates coseismic and viscoelastic ΔCFS induced by the three proceeding
 292 Yutian earthquakes.

293

294 From Table 1, at the hypocenter of the 12YT, the static and viscoelastic ΔCFS induced by
 295 08YT are smaller (approximately 10^{-3} to 10^{-4} MPa) than the triggering threshold (0.01 MPa),
 296 implying that the stress interaction between these two events is weak. At the hypocenter of the
 297 14YT, the static and viscoelastic ΔCFS induced by the 08YT (0.0036 MPa) are smaller than

298 the triggering threshold (0.01 MPa), which implies a weak interaction. The static and
299 viscoelastic ΔCFS induced by the 12YT on the 14YT are insignificant (approximately 10^{-4}
300 MPa), implying that the stress interaction between them is very weak. For the 20YT, the
301 ΔCFS induced by the 08YT is small (approximately 10^{-3} MPa), the ΔCFS induced by the
302 12YT is larger (approximately 10^{-2} MPa) than the triggering threshold, and the ΔCFS induced
303 by the 14YT is noticeable (approximately 10^{-1} MPa). These findings imply that the proceeding
304 Yutian earthquakes contributed to the occurrence of the 20YT. The largest triggering
305 contribution comes from the 14YT (approximately $71\% \approx 0.10523/0.1477$).

306



308 Figure 3 Spatial distribution of ΔCFS at the hypocenter of the 20YT induced by the four
309 Yutian earthquakes. (a), (d), (g) and (j) show static (coseismic) ΔCFS induced by the 08YT,
310 12YT, 14YT and 20YT. (b), (e), (h) and (k) show postseismic ΔCFS induced by the 08YT,
311 12YT, 14YT and 20YT. (c), (f), (i) and (l) show the combined (coseismic and postseismic)
312 ΔCFS induced by the 08YT, 12YT, 14YT and 20YT. (m) Combined ΔCFS induced by all
313 three proceeding Yutian earthquakes (08YT, 12YT and 14YT). (n) Combined ΔCFS induced
314 by all four Yutian earthquakes (08YT, 12YT, 14YT and 20YT) after one year of occurrence of
315 20YT. The black lines represent major faults, black stars indicate 08YT, 12YT and 14YT, and
316 yellow star shows location of 20YT. The resolving depth is 15 km and the strike, dip, and rake
317 angles are 213° , 52° , and -66° (GCMT), respectively.

318

319 The triggering contribution from the 08YT, 12YT and 14YT to the 20YT can also be clearly
320 identified from the spatial distribution of ΔCFS (Figure 3). From Figure 3a-3g, the epicenter
321 of the 20YT always falls into the positive zone of ΔCFS , which is similar to the results of *He*
322 *et al.* (2020). *He et al.* (2020) only calculated coseismic ΔCFS ; the spatial distribution of
323 ΔCFS induced by the 08YT, 12YT and 14YT (Figure 12 in their paper) is different in this
324 study (Figure 3m and 3n) in several regions, which are dominated by a large postseismic
325 ΔCFS from the 08YT (Figure 3b). The uncertainties of ΔCFS impacted by resolving depth,
326 receiver fault parameters and friction coefficient are also investigated in the Supplementary
327 Information (Tables S2-S3, Figures S5-S7), and the results are similar. The 08YT and 14YT
328 generated a wider spatial stress disturbance than the 12YT due to their larger magnitudes. It is
329 also interesting that several faults between the epicenters of 08YT and 20YT experience a
330 positive ΔCFS induced by the 08YT and a negative ΔCFS induced by the 14YT at the same
331 time. The seismic hazard in this region may receive more research attention.

332

333 **4. Discussion**

334 4.1 Uncertainties of calculations of ΔCFS

335 Large uncertainties in the calculations of ΔCFS caused by nonunique solutions of the source
336 slip distribution and poorly constrained parameters (e.g., friction coefficient and resolving

337 depth) may weaken the results based on ΔCFS (Jia *et al.*, 2018; Steacy *et al.*, 2004; Wang *et*
338 *al.*, 2014a). Jia *et al.* (2018) have shown that large uncertainties in ΔCFS may lead to different
339 or even conflicting results in the case of the 2008 Wenchuan and 2017 Jiuzhaigou earthquakes
340 in China. One way to minimize uncertainties is properly choosing source models and
341 parameters. On the other hand, ranges of uncertainties are also investigated by calculating
342 ΔCFS using different possible parameters. As described in the calculation of ΔCFS , the
343 coseismic slip models of the 08YT (Elliott *et al.*, 2010) and 14YT (Zhang *et al.*, 2014) are
344 chosen because they are the best choices for representative models of source slip distributions.
345 For the 12YT, there is no other way to use a better source model than the synthetic slip model
346 estimated from the empirical relations of Wells and Coppersmith (1994). The uncertainties due
347 to different choices of friction coefficient and resolving depth are investigated (Tables S2-S3,
348 Figures S5-S7). Pollitz *et al.* (2006) explored coseismic and postseismic stress changes
349 following the 26 December 2004 Sumatra-Andaman and 28 March 2005 Nias earthquakes
350 using different friction coefficients and found that the CFS changes are similar for values of
351 μ' ranging from 0 to 0.8. In this study, a higher (0.8) or lower (0.2) value of the friction
352 coefficient does not noticeably influence the results of ΔCFS for this case (Tables S2 and S3,
353 Figures S5 and S6). Calculations using different resolving depths (10 km and 15 km) show that
354 the resolving depth also does not change the results of ΔCFS much (Figure S7). Thus, our
355 conclusions based on ΔCFS are still valid considering the uncertainties. Because the focal
356 mechanisms of the 20YT from different data sources (e.g., GCMT and NEIC-USGS) are similar,
357 uncertainties of ΔCFS using different receiver fault parameters (strike, dip and rake) are small
358 (Figure S8).

359

360 4.2 Validation of the Coulomb failure hypothesis

361 Stress interactions among multiple faults in a local-scale region provide a good opportunity to
362 test the Coulomb failure hypothesis. Previous case studies have shown some successful
363 examples from the view of stress transfer (Freed and Lin, 2001; Jia *et al.*, 2014; Jia *et al.*, 2018;
364 Pope and Mooney, 2020; Quigley *et al.*, 2016). However, as mentioned above, calculations of
365 ΔCFS suffer large uncertainties, and the results are subjective to some degree (e.g., choices of

366 source models and parameters are subjective). It is necessary to verify the results of ΔCFS
367 from another perspective. Statistical insight (e.g., ETAS model) provides a good cross reference
368 for its objectivity and small uncertainties. Background probabilities estimated from the formula
369 (1) provide information on whether earthquakes are triggered aftershocks or tectonic
370 background events. A low value (close to zero) of background probability indicates a triggered
371 event, which usually experiences a positive ΔCFS induced by other major earthquakes. A high
372 background probability value (close to 1.0) represents an independent event, which usually has
373 no stress interaction with other earthquakes and results from tectonic loading. *Jia et al.* (2018)
374 conducted a statistical analysis in the Jiuzhaigou region, southwestern China, to clarify the
375 triggering relationship of the 2008 Wenchuan and 2017 Jiuzhaigou earthquakes, which cannot
376 be well deduced from the results of ΔCFS . In this study, the background probability of the
377 12YT (0.97) coincides with the positive ΔCFS calculated on its hypocenter induced by the
378 other major earthquakes (-1.5×10^{-4} MPa). Background probabilities of the 14YT (1.5×10^{-3})
379 and 20YT (8.7×10^{-5}) coincide with positive ΔCFS calculated on their hypocenters induced
380 by the proceeding Yutian earthquakes (0.0036 MPa for the 14YT and 0.18 MPa for the 20YT).
381 From these two different kinds of perspectives, the stress interaction among multiple faults or
382 earthquakes can be comprehensively investigated.

383

384 **5. Conclusion**

385 The June 26, 2020 Mw 6.3 Yutian earthquake, which occurred on the western boundary of the
386 Bayan Har block, is the fourth M6+ earthquake in this region since the occurrence of the 08YT.
387 We have investigated the stress interaction among the 08YT, 12YT, 14YT and 20YT by
388 applying the ETAS model and calculating ΔCFS . The joint application of these two
389 independent methods provides insight into earthquake triggering mechanisms from both
390 physics-based and statistics-based views in our study region and worldwide. From a statistical
391 view, the background probabilities of the 08YT, 12YT, 14YT and 20YT are 0.87, 0.97, $1.5 \times$
392 10^{-3} and 8.7×10^{-5} , respectively, implying that the 08YT and 12YT are more similar to
393 background earthquakes and that the 14YT and 20YT are triggered events. The epicenters of
394 the 08YT, 12YT, 14YT and 20YT are located in the highest background seismicity areas
395 (approximately $0.1 M \geq 3.5$ events/degree²/yr), which is a complex stepover zone with multiple

396 normal faults. From a physical view, the combined ΔCFS induced by the proceeding Yutian
397 earthquakes on hypocenters of the 12YT, 14YT and 20YT are -1.50×10^{-4} , 3.6×10^{-3} and 1.5
398 $\times 10^{-1}$ MPa, respectively. These two kinds of evidence are consistent with each other, implying
399 a triggering effect from the 08YT to the 14YT and the 20YT. Thus, a cross check of using the
400 ETAS model and calculating ΔCFS together provides a robust and reliable way to investigate
401 earthquake triggering mechanisms.

402

403 **Acknowledgement**

404 The catalog used in this study is from the China Earthquake Data Center (CEDC,
405 <http://data.earthquake.cn/index.html>). The PSGRN/PSCMP code is provided by Prof.
406 Rongjiang Wang. We benefit from discussion with Fuqiang Shi and Hurong Duan. We
407 appreciate the comments and suggestions of two anonymous reviewers and the editor Lucy
408 Flesch, which greatly improved this article. This research is jointly supported by the National
409 Key R&D Program of China (2018YFC1503400), the National Natural Science Foundation of
410 China projects (41804048, U2039204), the China Seismic Experimental Site (2019CSES0106),
411 the China Postdoctoral Science Foundation (2020M673469), and the Fundamental Research
412 Funds for the Central Universities (3102019ZDHKY12). Generic Mapping Tool mapping
413 software (*Wessel and Smith*, 1991) is used to prepare some figures.

414

415

416 **References**

- 417 Agata, R., S. D. Barbot, K. Fujita, M. Hyodo, T. Iinuma, R. Nakata, T. Ichimura, and T. Hori (2019),
418 Rapid mantle flow with power-law creep explains deformation after the 2011 Tohoku mega-quake,
419 *Nature communications*, *10*(1), 1-11.
- 420 Bie, L., and I. Ryder (2014), Recent seismic and aseismic activity in the Ashikule stepover zone, NW
421 Tibet, *Geophysical Journal International*, *198*(3), 1632-1643.
- 422 Cattania, C., S. Hainzl, L. Wang, B. Enescu, and F. Roth (2015), Aftershock triggering by postseismic
423 stresses: A study based on Coulomb rate - and - state models, *Journal of Geophysical Research: Solid*
424 *Earth*, *120*(4), 2388-2407.
- 425 Elliott, J. R., R. J. Walters, P. C. England, J. A. Jackson, Z. Li, and B. Parsons (2010), Extension on the
426 Tibetan plateau: recent normal faulting measured by InSAR and body wave seismology, *Geophysical*
427 *Journal International*, *183*(2), 503-535.
- 428 Freed, A. M. (2005), Earthquake triggering by static, dynamic, and postseismic stress transfer, *Annu. Rev.*
429 *Earth Planet. Sci.*, *33*, 335-367.

430 Freed, A. M. (2007), Afterslip (and only afterslip) following the 2004 Parkfield, California, earthquake,
431 *Geophysical Research Letters*, 34(6).

432 Freed, A. M., and J. Lin (2001), Delayed triggering of the 1999 Hector Mine earthquake by viscoelastic
433 stress transfer, *Nature*, 411(6834), 180-183, doi:10.1038/35075548.

434 Gomberg, J., P. Reasenberg, P. I. Bodin, and R. Harris (2001), Earthquake triggering by seismic waves
435 following the Landers and Hector Mine earthquakes, *Nature*, 411(6836), 462-466.

436 Harris, R. A. (1998), Introduction to Special Section: Stress Triggers, Stress Shadows, and Implications
437 for Seismic Hazard, *Journal of Geophysical Research*, 103(10), 24347-24358.

438 Harris, R. A., and R. W. Simpson (1996), In the shadow of 1857—the effect of the Great Ft. Tejon
439 Earthquake on subsequent earthquakes in southern California, *Geophysical Research Letters*, 23(3), 229–
440 232.

441 He, P., M. Wang, Q. Wang, and Z. Shen (2018), Rheological structure of lithosphere in northern Tibet
442 inferred from postseismic deformation modeling of the 2001 Mw 7.8 Kokoxili earthquake, *Chinese
443 Journal of Geophysics-Chinese Edition*, 61(2), 531-544.

444 He, P., Y. Wen, K. Ding, and C. Xu (2020), Normal Faulting in the 2020 Mw 6.2 Yutian Event:
445 Implications for Ongoing E–W Thinning in Northern Tibet, *Remote Sensing*, 12(18), 3012.

446 Helmstetter, A., and B. E. Shaw (2009), Afterslip and aftershocks in the rate - and - state friction law,
447 *Journal of Geophysical Research: Solid Earth*, 114(B1).

448 Hill, D., and S. Prejean (2007), Dynamic triggering, *Treatise on Geophysics*, 4, 257-292.

449 Hughes, K. L., T. Masterlark, and W. D. Mooney (2010), Poroelastic stress-triggering of the 2005 M8.7
450 Nias earthquake by the 2004 M9.2 Sumatra–Andaman earthquake, *Earth and Planetary Science Letters*,
451 293(3-4), 289-299.

452 Jia, K., S. Zhou, and R. Wang (2012), Stress Interactions within the Strong Earthquake Sequence from
453 2001 to 2010 in the Bayankala Block of Eastern Tibet, *Bulletin of the Seismological Society of America*,
454 102(5), 2157-2164.

455 Jia, K., S. Zhou, J. Zhuang, and C. Jiang (2014), Possibility of the Independence between the 2013
456 Lushan Earthquake and the 2008 Wenchuan Earthquake on Longmen Shan Fault, Sichuan, China,
457 *Seismological Research Letters*, 85(1), 60-67, doi:10.1785/0220130115.

458 Jia, K., S. Zhou, J. Zhuang, C. Jiang, Y. Guo, Z. Gao, and S. Gao (2018), Did the 2008 Mw 7.9 Wenchuan
459 earthquake trigger the occurrence of the 2017 Mw 6.5 Jiuzhaigou earthquake in Sichuan, China?, *Journal
460 of Geophysical Research: Solid Earth*, 123(4), 2965-2983.

461 Jiang, C., L. Han, and L. Guo (2014), Parameter Characteristics in the Early Period of Three Earthquake
462 Sequences in the Yutian, Xinjiang Since 2008, *Acta Seis-mologia Sinica*, 36(2), 165-174.

463 Jonsson, S., P. Segall, R. Pedersen, and G. Björnsson (2003), Post-earthquake ground movements
464 correlated to pore-pressure transients, *Nature*, 424(6945), 179-183.

465 Kroll, K. A., K. B. Richards - Dinger, J. H. Dieterich, and E. S. Cochran (2017), Delayed seismicity rate
466 changes controlled by static stress transfer, *Journal of Geophysical Research: Solid Earth*, 122(10),
467 7951-7965.

468 Li, Y., L. Chen, S. Liu, S. Yang, X. Yang, and G. Zhang (2015), Coseismic Coulomb stress changes
469 caused by the Mw6.9 Yutian earthquake in 2014 and its correlation to the 2008 Mw7.2 Yutian earthquake,
470 *Journal of Asian Earth Sciences*, 105, 468-475.

471 Liu, S., Z.-K. Shen, R. Bürgmann, and S. Jónsson (2021), Thin crème brûlée rheological structure for the
472 Eastern California Shear Zone, *Geology*, 49(2), 216-221.

473 Masuti, S., S. D. Barbot, S. I. Karato, L. Feng, and P. Banerjee (2016), Upper-mantle water stratification

474 inferred from observations of the 2012 Indian Ocean earthquake, *Nature*, 538(7625), 373.

475 McCloskey, J., S. S. Nalbant, and S. Steacy (2005), Earthquake risk from co-seismic stress, *Nature*,
476 434(7031), 291-291.

477 Meng, X., and Z. Peng (2014), Seismicity rate changes in the Salton Sea Geothermal Field and the San
478 Jacinto Fault Zone after the 2010 Mw 7.2 El Mayor-Cucapah earthquake, *Geophysical Journal
479 International*, 197(3), 1750-1762.

480 Nur, A., and G. Mavko (1974), Postseismic Viscoelastic Rebound, *Science*, 183(4121), 204-206.

481 Ogata, Y. (1998), Space-Time Point-Process Models for Earthquake Occurrences, *Annals of the Institute
482 of Statistical Mathematics*, 50(2), 379-402, doi:10.1023/A:1003403601725.

483 Ogata, Y. (2004), Space-time model for regional seismicity and detection of crustal stress changes,
484 *Journal of Geophysical Research*, 109(B3), 235-273.

485 Ogata, Y., and J. Zhuang (2006), Space-time ETAS models and an improved extension, *Tectonophysics*,
486 413(1-2), 13-23, doi:10.1016/j.tecto.2005.10.016.

487 Parsons, T. (2002), Global Omori law decay of triggered earthquakes: Large aftershocks outside the
488 classical aftershock zone, *Journal of Geophysical Research*, 107(B9), 2199, doi:10.1029/2001JB000646.

489 Peña, C., O. Heidbach, M. Moreno, J. Bedford, M. Ziegler, A. Tassara, and O. Oncken (2019), Role of
490 lower crust in the postseismic deformation of the 2010 Maule earthquake: Insights from a model with
491 power-law rheology, *Pure and Applied Geophysics*, 176(9), 3913-3928.

492 Peña, C., O. Heidbach, M. Moreno, J. Bedford, M. Ziegler, A. Tassara, and O. Oncken (2020), Impact of
493 power-law rheology on the viscoelastic relaxation pattern and afterslip distribution following the 2010
494 Mw 8.8 Maule earthquake, *Earth and Planetary Science Letters*, 542, 116292.

495 Pollitz, F. F., P. Banerjee, R. Bürgmann, M. Hashimoto, and N. Choosakul (2006), Stress changes along
496 the Sunda trench following the 26 December 2004 Sumatra - Andaman and 28 March 2005 Nias
497 earthquakes, *Geophysical research letters*, 33(6).

498 Pollitz, F. F., and C. Cattania (2017), Connecting crustal seismicity and earthquake - driven stress
499 evolution in Southern California, *Journal of Geophysical Research: Solid Earth*, 122(8), 6473-6490.

500 Pope, N., and W. D. Mooney (2020), Coulomb stress models for the 2019 Ridgecrest, California
501 earthquake sequence, *Tectonophysics*, 791, 228555.

502 Quigley, M. C., M. W. Hughes, B. A. Bradley, S. van Ballegooy, C. Reid, J. Morgenroth, T. Horton, B.
503 Duffy, and J. R. Pettinga (2016), The 2010–2011 Canterbury earthquake sequence: Environmental effects,
504 seismic triggering thresholds and geologic legacy, *Tectonophysics*, 672, 228-274.

505 Ramos, M. D., J. C. Neo, P. Thakur, Y. Huang, and S. Wei (2020), Stress Changes on the Garlock fault
506 during and after the 2019 Ridgecrest Earthquake Sequence, *Bulletin of the Seismological Society of
507 America*.

508 Reasenberg, P. A., and R. W. Simpson (1992), Response of regional seismicity to the static stress change
509 produced by the loma prieta earthquake, *Science*, 255(5052), 1687.

510 Steacy, S., J. Gomberg, and M. Cocco (2005), Introduction to special section: Stress transfer, earthquake
511 triggering, and time-dependent seismic hazard, *Journal of Geophysical Research*, 110(B5),
512 doi:10.1029/2005JB003692.

513 Steacy, S., D. Marsan, S. S. Nalbant, and J. McCloskey (2004), Sensitivity of static stress calculations to
514 the earthquake slip distribution, *Journal of Geophysical Research: Solid Earth (1978–2012)*, 109(B4).

515 Stein, R. S. (1999), The role of stress transfer in earthquake occurrence, *Nature*, 402(6762), 605-609,
516 doi:10.1038/45144.

517 Tapponnier, P., X. Zhiqin, F. Roger, B. Meyer, N. Arnaud, G. Wittlinger, and Y. Jingsui (2001), Oblique

518 stepwise rise and growth of the Tibet Plateau, *science*, 294(5547), 1671-1677.

519 Taylor, M., and A. Yin (2009), Active structures of the Himalayan-Tibetan orogen and their relationships
520 to earthquake distribution, contemporary strain field, and Cenozoic volcanism Active structures on the
521 Tibetan plateau and surrounding regions, *Geosphere*, 5(3), 199-214.

522 Toda, S., R. S. Stein, G. C. Beroza, and D. Marsan (2012), Aftershocks halted by static stress shadows,
523 *Nature Geoscience*, 5(6), 410-413.

524 Toda, S., R. S. Stein, K. Richards-Dinger, and S. B. Bozkurt (2005), Forecasting the evolution of
525 seismicity in southern California: Animations built on earthquake stress transfer, *Journal of Geophysical*
526 *Research*, 110(B5), doi:10.1029/2004JB003415.

527 Tung, S., and T. Masterlark (2018), Delayed poroelastic triggering of the 2016 October Visso earthquake
528 by the August Amatrice earthquake, Italy, *Geophysical Research Letters*, 45(5), 2221-2229.

529 Wan, Y., and Z.-K. Shen (2010), Static Coulomb stress changes on faults caused by the 2008 Mw 7.9
530 Wenchuan, China earthquake, *Tectonophysics*, 491(1–4), 105-118, doi:10.1016/j.tecto.2010.03.017.

531 Wang, J., C. Xu, J. T. Freymueller, and Z. Li (2017), Probing Coulomb stress triggering effects for a Mw
532 > 6.0 earthquake sequence from 1997 to 2014 along the periphery of the Bayan Har block on the
533 Tibetan Plateau, *Tectonophysics*, 694, 249-267, doi:<https://doi.org/10.1016/j.tecto.2016.11.009>.

534 Wang, J., C. Xu, J. T. Freymueller, Z. Li, and W. Shen (2014a), Sensitivity of Coulomb stress change to
535 the parameters of the Coulomb failure model: A case study using the 2008 M w 7.9 Wenchuan earthquake,
536 *Journal of Geophysical Research*, 119(4), 3371–3392.

537 Wang, K., and Y. Fialko (2018), Observations and Modeling of Coseismic and Postseismic Deformation
538 Due To the 2015 Mw 7.8 Gorkha (Nepal) Earthquake, *Journal of Geophysical Research Solid Earth*.

539 Wang, R., F. Lorenzo-Martín, and F. Roth (2006), PSGRN/PSCMP—A new code for calculating co-and
540 post-seismic deformation, geoid and gravity changes based on the viscoelastic-gravitational dislocation
541 theory, *Computers and Geosciences*, 32(4), 527-541.

542 Wang, Y., F. Wang, M. Wang, Z. K. Shen, and Y. Wan (2014b), Coulomb Stress Change and Evolution
543 Induced by the 2008 Wenchuan Earthquake and its Delayed Triggering of the 2013 Mw 6.6 Lushan
544 Earthquake, *Seismological Research Letters*, 85(1), 52-59.

545 Wells, D. L., and K. J. Coppersmith (1994), New empirical relationships among magnitude, rupture
546 length, rupture width, rupture area, and surface displacement, *Bulletin of the seismological Society of*
547 *America*, 84(4), 974-1002.

548 Wessel, P., and W. H. F. Smith (1991), Free software helps map and display data, *Eos Trans. AGU*, 72(41),
549 441-446, doi:10.1029/90eo00319.

550 Xiong, X., B. Shan, Y. Zheng, and R. Wang (2010), Stress transfer and its implication for earthquake
551 hazard on the Kunlun Fault, Tibet, *Tectonophysics*, 482(1–4), 216-225, doi:10.1016/j.tecto.2009.07.020.

552 Xu, X., X. Tan, G. Yu, G. Wu, W. Fang, J. Chen, H. Song, and J. Shen (2013), Normal-and oblique-slip
553 of the 2008 Yutian earthquake: evidence for eastward block motion, northern Tibetan Plateau,
554 *Tectonophysics*, 584, 152-165.

555 Zhang, P., Q. Deng, G. Zhang, J. Ma, W. Gan, W. Min, F. Mao, and Q. Wang (2003), Active tectonic
556 blocks and strong earthquakes in the continent of China, *Science in China Series D: Earth Sciences (in*
557 *Chinese)*, 46(2), 13-24.

558 Zhang, Y., L.-s. Xu, Y.-T. Chen, and R.-j. Wang (2014), Fast inversion for the rupture process of the 12
559 February 2014 Yutian MW6. 9 earthquake: Discussion on the impacts of focal mechanisms on rupture
560 process inversions, *Acta Seismologica Sinica*, 36(2), 159-164.

561 Zhao, L., L. Zhao, and X. Xie (2016), Static Coulomb stress changes and seismicity rate in the source

562 region of the 12 February, 2014 M W 7.0 Yutian earthquake in Xinjiang, China, *Chinese Journal of*
563 *Geophysics*, 3732-3743.

564 Zhuang, J., C.-P. Chang, Y. Ogata, and Y.-I. Chen (2005), A study on the background and clustering
565 seismicity in the Taiwan region by using point process models, *J. Geophys. Res.*, 110(B5),
566 doi:10.1029/2004jb003157.

567 Zhuang, J., Y. Ogata, and D. Vere-Jones (2004), Analyzing earthquake clustering features by using
568 stochastic reconstruction, *Journal of Geophysical Research: Solid Earth*, 109(B5), B05301,
569 doi:10.1029/2003JB002879.

570